Linear Analysis of a Two-Parachute System Undergoing Pendulum Motion

Carlos M. Roithmayr*, Jim Beaty†, Jing Pei‡
NASA Langley Research Center, Hampton, Virginia, 23681

Richard L. Barton§, and Daniel A. Matz¶
NASA Johnson Space Center, Houston, Texas, 77058

April 8, 2019

Motion resembling that of a pendulum undergoing large-amplitude oscillation was observed during a series of flight tests of an unoccupied Orion Capsule Parachute Assembly System (CPAS) drop-test vehicle. Large excursions away from vertical by the capsule could cause it to strike the ground or ocean at a large angle with respect to vertical, with an undesirable attitude with respect to heading, or with a large horizontal or vertical speed. These conditions are to be avoided because they would endanger the occupants of the capsule in an actual mission. Pendulum motion is intimately related to a parachute's aerodynamic normal force coefficient, which is a nonlinear function of angle of attack. An analytical investigation of the dynamics of pendulum motion is undertaken with the aid of a simplified model of the physical system and the assumption that the normal force coefficient is a linear function of angle of attack in the neighborhood of a value corresponding to stable equilibrium. The analysis leads to a simple relationship for the location of a pivot point, which provides insights that are consistent with previous studies.

I. Introduction

As discussed in Ref. [1], a series of flight tests was conducted to characterize the performance of the Orion Multi Purpose Crew Vehicle (MPCV) parachute cluster. It is apparent in multiple flight tests that the system consisting of the payload and two parachutes can undergo pendulum motion in which the payload makes large excursions from vertical. The pendulum motion can result in the capsule striking the ground or ocean at a large angle with respect to vertical, with an undesirable attitude with respect to heading, or with a large horizontal or vertical speed, all of which is highly objectionable. Pendulum motion is not observed when the payload is supported by the nominal configuration of three parachutes. In Ref. [1] Ray and Machín describe the pendulum motion observed during flight testing and summarize a series of studies performed in an attempt to understand the causes of the phenomenon. The period of oscillation and location of the system's pivot point are determined from post-flight analysis. The paper also discusses modeling and testing that was undertaken to understand the underlying issues.

Over the past 50 years, a number of analytical, numerical, and experimental investigations have been performed with the goal of understanding parachute system pitch-plane dynamics (for example, Refs. [2]–[5]). Several insightful observations are made in Refs. [2] and [5]. First, aerodynamic forces acting on the capsule can be neglected in dynamic modeling. Second, the system can be made less susceptible to pendulum motion by increasing the parachute normal force coefficient slope at the trim angle of attack and

*Senior Aerospace Engineer, Vehicle Analysis Branch
†Senior Aerospace Engineer, Vehicle Analysis Branch (retired)
‡Aerospace Engineer, Vehicle Analysis Branch
§Branch Chief, Aeroscience Branch (retired)
¶Aerospace Engineer, Flight Mechanics and Trajectory Design Branch

by decreasing the parachute drag coefficient. Third, pendulum motion is exacerbated by decreasing the payload mass and by the increased atmospheric density at lower altitudes. These findings are substantiated by performing Computational Fluid Dynamics (CFD) analysis of the Apollo and MPCV main parachute configurations. As discussed in Refs. [6] and [7], the static stability characteristics of a parachute can be improved by increasing the porosity. However, the resulting decrease in drag for the nominal three-parachute configuration increases the steady-state descent rate.

The lower portion of Fig. 1 shows aerodynamic normal force coefficient, C_N, as a nonlinear function of angle of attack, α, for a parachute. As discussed in Ref. [6], the dashed and solid curves correspond to stable and unstable parachutes, respectively. In the first case, C_N is approximately equal to zero between -10 deg and 10 deg, whereas in the second case, $C_N = 0$ at three distinct points of equilibrium. Pendulum motion is associated with an unstable parachute; hence, the analysis presented in this paper is confined to parachutes characterized by the solid curve. Other features of Fig. 1 are discussed in Sec. III.E.

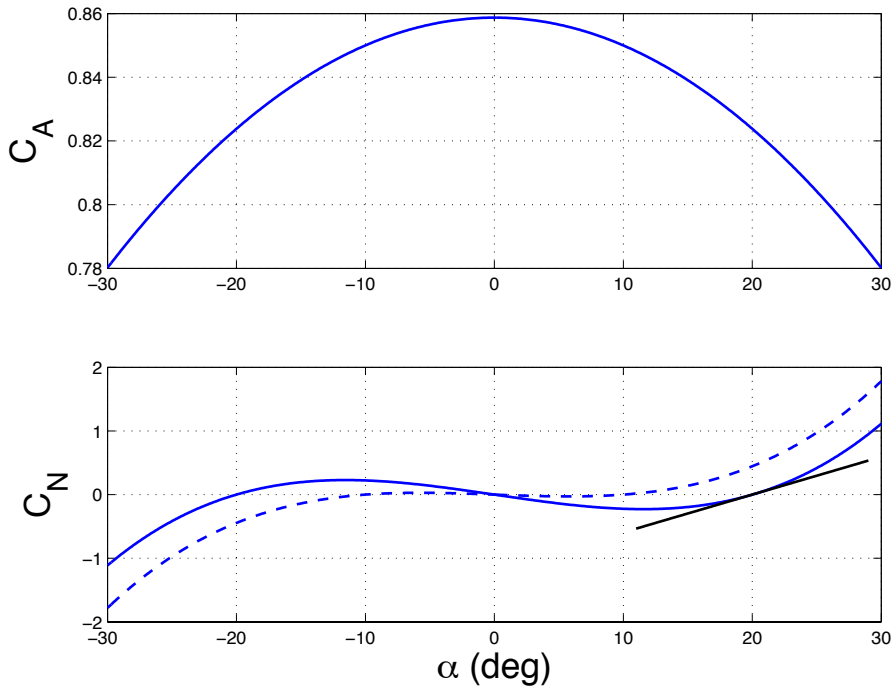

Figure 1. C_A and C_N, Nonlinear Functions of α.

An analytical investigation of the dynamics of pendulum motion is undertaken by assuming that C_N is a linear function of α in the neighborhood of a stable equilibrium point. The system composed of a capsule and two parachutes is modeled as a simple dumbbell performing planar motion. For small-amplitude oscillations, the rotational equation of motion is found to have the form of the second-order linear differential equation governing damped, free vibrations, and a general solution of the differential equation is given. A point on the dumbbell whose trajectory is nearly a straight line for undamped, small-amplitude oscillations is identified. The distance from this pivot point to the capsule is of interest because the capsule moves as though that distance is the length of a simple pendulum.

In the case of a simple pendulum, the length of the string between the pivot point and pendulum bob determines the distance traveled by the bob on a circular arc as the pendulum swings. The length of the string also determines the period of oscillations. Analogously, the distance from the pivot point to the capsule is an important parameter in capsule-parachute pendulum motion. When this distance is minimized, undesirable swinging motion of the capsule is also minimized. The main contribution of the present paper is the development of an analytical relationship for the location of the pivot point as a function of the parachute normal force coefficient slope, axial force coefficient, payload mass, parachute dry mass, and mass of the air entrapped in a parachute. So far as the authors are aware, this result has not been reported in the

literature, including Refs. [2] and [3] that contain analysis in which C_N is treated as a linear function of α. Examination of the analytic relationship confirms the insightful observations made in Refs. [2] and [5] – [7]. The analysis in the paper is focused on what occurs once pendulum motion has commenced; the causes of pendulum motion are not addressed.

The remainder of the paper is organized as follows. A three-dimensional model of a capsule and two parachutes is discussed in Sec. II. A simplified planar model of the system is presented in Sec. III and used as the basis for an analytical study of the fundamental dynamics of pendulum motion. In Sec. IV, numerical results are provided to demonstrate that the acceleration of the pivot point is nearly zero for several values of aerodynamic parameters, and the trajectory of the pivot point is shown to be nearly a straight line in each case. Time histories of the horizontal and vertical projections of the velocities of the payload and parachutes are provided. Results obtained with the dumbbell model are compared with results obtained from numerical simulations based on more sophisticated models of the capsule and parachutes. Conclusions are presented in Sec. V.

II. Model in Three Dimensions

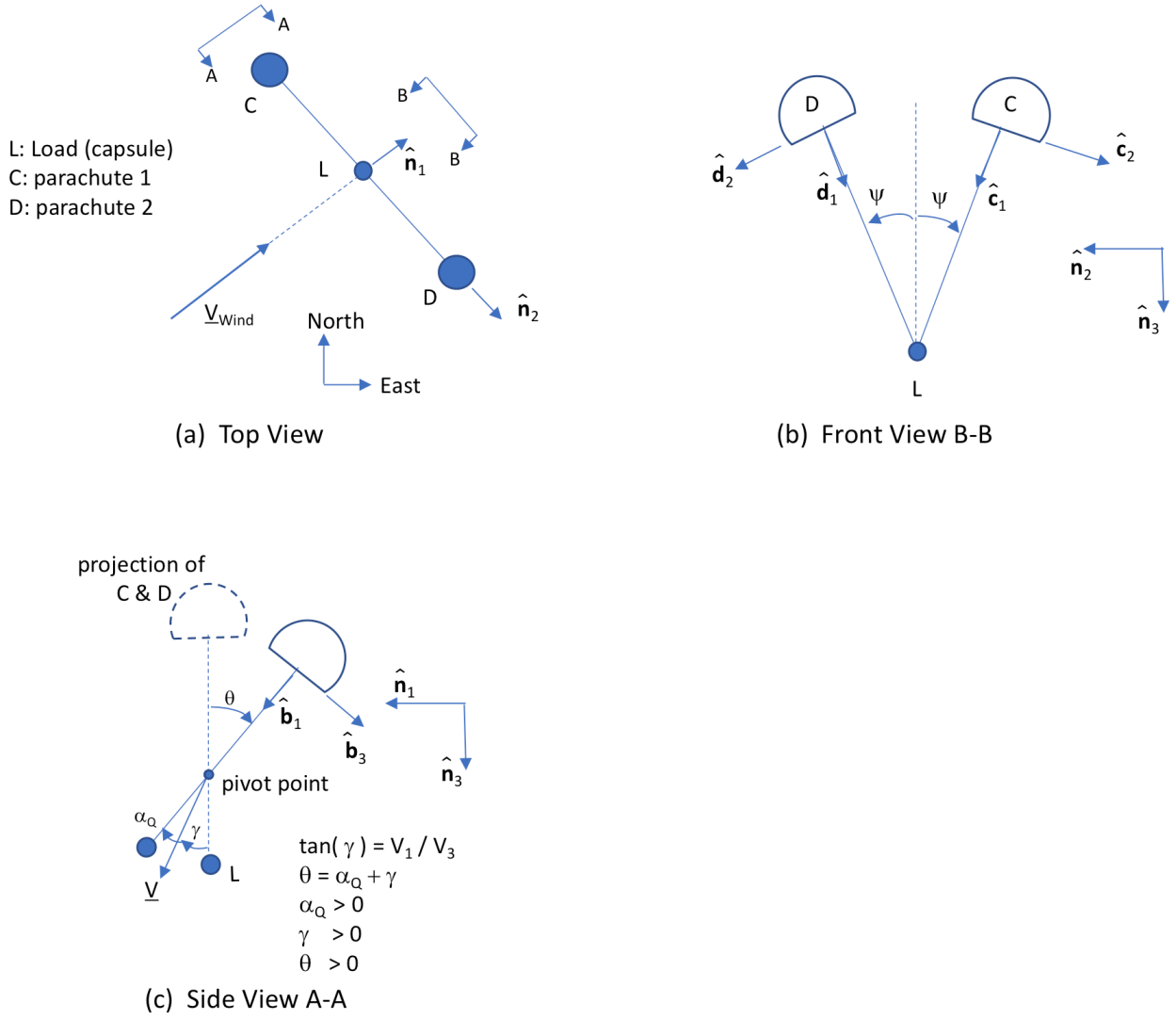

Figure 2. Geometry of Capsule and Parachutes.

A system consisting of a capsule (or load) suspended from two parachutes is described in three dimensions.

The description of the system and its behavior is applicable when the angle of attack of both parachutes is in the neighborhood of a stable equilibrium point. Various views of the system's configuration are presented in Fig. 2. Figure 2(a), upper left, shows an overhead view of the system in the steady state. Without loss of generality, a wind is depicted as blowing from the southwest to the northeast. The plane containing the two parachutes, C and D, and the capsule, L, is perpendicular to the direction of the wind, as discussed in Ref. [1]. The views labeled B-B and A-A in Fig. 2(a) are of planes perpendicular and parallel to the direction of the wind, respectively. A front view B-B is shown in Fig. 2(b). Side view A-A is presented in Fig. 2(c).

Throughout Fig. 2, $\hat{\mathbf{n}}_1$, $\hat{\mathbf{n}}_2$, and $\hat{\mathbf{n}}_3$ constitute a set of right-handed orthogonal unit vectors fixed in a Newtonian reference frame N. Unit vector $\hat{\mathbf{n}}_3$ is vertical, and directed downward. $\hat{\mathbf{n}}_2$ and $\hat{\mathbf{n}}_3$ lie in the plane perpendicular to the wind direction (view B-B), whereas $\hat{\mathbf{n}}_1$ and $\hat{\mathbf{n}}_3$ lie in the plane parallel to the wind direction (view A-A). Pendulum motion occurs in the latter plane, as discussed in Sec. III.

During equilibrium descent, the resultant of the forces acting on C, D, and L is zero. Aerodynamic force acting on capsule L is neglected, as suggested in Ref. [2]. The aerodynamic side force applied to parachute D in the direction of $\hat{\mathbf{n}}_2$ is equal in magnitude and opposite in direction to the aerodynamic side force applied to parachute C. The lateral separation of C and D shown in Fig. 2(b) results from aerodynamic side force trim and parachute proximity aerodynamic effects. The lines that join L to C and to D are symmetric with respect to vertical; the angle between each line and the vertical is ψ. The gravitational force (weight) acting in the direction of $\hat{\mathbf{n}}_3$, due to the mass of L and the dry masses of C and D, is equal in magnitude and opposite in direction to the resultant of the vertical aerodynamic forces acting on C and D. The equilibrium descent rate is denoted by V_3.

The dashed hemisphere and vertical line in Fig. 2(c) show the configuration of the system during equilibrium descent, in the absence of pendulum motion. The dashed hemisphere represents the projection of parachutes C and D onto the plane parallel to the wind direction. The projection is directly above the load when the pendulum swing angle, θ, is zero. When the parachutes reach steady-state trim at a stable trim angle of attack α_0, with θ and its time derivative $\dot{\theta}$ both equal to zero, the aerodynamic force in the horizontal direction, $\hat{\mathbf{n}}_1$, produces a constant lateral speed denoted by V_1. Thus, during equilibrium descent, all points of the system have zero acceleration in N and therefore a constant velocity in N, $\mathbf{V} = V_1\hat{\mathbf{n}}_1 + V_3\hat{\mathbf{n}}_3$, where V_3 is the steady-state descent rate. The flight path angle γ, defined such that $\tan\gamma = V_1/V_3$, is therefore constant and equal to the negative of α_0 as a direct consequence of the parachutes having reached a trim angle of attack. It is worth noting that γ is defined here (for convenience) to be zero when $V_1 = 0$, and that this definition differs from the usual aerospace convention. When V_1 is positive, γ is defined to be positive, as indicated in Fig. 2(c). During pendulum motion there exists a pivot point whose acceleration in N is nearly zero, as discussed in Sec. III.G. The pendulum swing angle, θ, is equal to the sum of γ and the angle of attack at the pivot point, α_Q. Figure 2(c) depicts a case in which $\gamma < \theta$, so that $\alpha_Q > 0$.

For the purposes of the present discussion, parachute C is regarded as a rigid body. In Fig. 2(b), unit vector $\hat{\mathbf{c}}_1$ is fixed in C, parallel to the riser line connecting parachute C to L, and it is directed toward L. Unit vector $\hat{\mathbf{c}}_2$ is also fixed in C, perpendicular to $\hat{\mathbf{c}}_1$. Per traditional aerodynamic definitions, the aerodynamic axial force is applied to C in the direction of $-\hat{\mathbf{c}}_1$, and the aerodynamic side force is applied in the direction of $\hat{\mathbf{c}}_2$. Similar statements can be made in connection with parachute D. In Fig. 2(c), unit vectors $\hat{\mathbf{b}}_1$ and $\hat{\mathbf{b}}_3$ are fixed in a reference frame corresponding to the projection of C and D onto the plane parallel to the wind direction. In keeping with traditional aerodynamic definitions, the resultant of aerodynamic axial forces acting on the two parachutes is applied in the direction of $-\hat{\mathbf{b}}_1$.

As discussed previously in connection with Fig. 2(b), the resultant of the aerodynamic side forces applied to the two parachutes is zero; the side forces do not play a part in the pendulum motion investigated in Sec. III. On the other hand, as will be seen, the resultant of the aerodynamic normal forces plays a significant role in pendulum dynamics. In what follows, the terms "normal force" and "aerodynamic normal force coefficient" (C_N, C_{N_α}, and $C_{N_{\dot{\alpha}}}$) refer to the aerodynamic characteristics of the two parachutes in the plane that is parallel to the wind direction as depicted in Fig. 2(c).

III. Planar Model

A dumbbell serves as a simplified model that can be used to study planar pendulum motion of a capsule and a pair of parachutes when their angle of attack is in the neighborhood of a stable equilibrium point. After the model is described in detail, kinematic analysis is performed to obtain expressions for the accelerations of the two particles that make up the dumbbell. The forces acting on the dumbbell are discussed in general

terms, and then a dynamical equation governing rotational motion is obtained. Detailed expressions are provided for the aerodynamic forces acting on the parachutes. For small-amplitude oscillations, the rotational equation of motion is found to have the form of the second-order linear differential equation governing damped, free vibrations, and a general solution of the differential equation is given. The section concludes with identification of a point on the dumbbell whose trajectory is nearly a straight line for undamped, small-amplitude oscillations. The distance from this pivot point to the capsule is of interest because the capsule moves as though that distance is the length of a simple pendulum.

A. Description of Planar Model

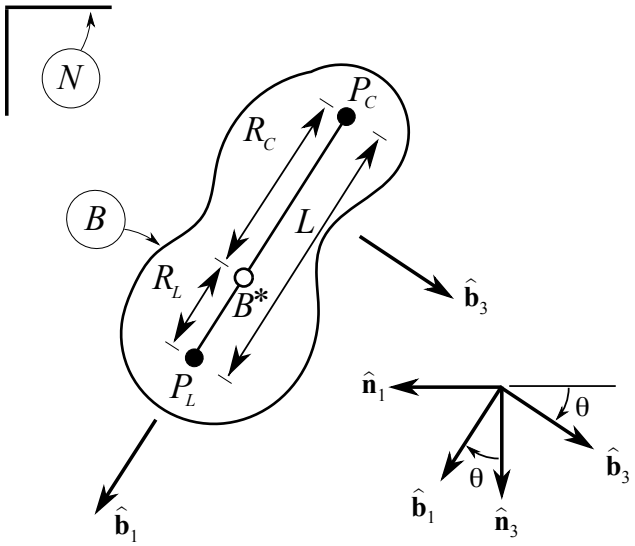

Figure 3. Rigid Body Containing Two Particles.

The three-dimensional system of interest is described in Sec. II. Clearly, the system is not a single rigid body. However, a great deal of insight into pendulum motion is gained by modeling the system as a simple dumbbell performing planar motion. The capsule is modeled as a particle rather than an extended rigid body. We adopt one of the simplifying assumptions in Ref. [2] and neglect aerodynamic force acting on the capsule. The two parachutes are treated as a single effective parachute, modeled as a particle in the plane parallel to the wind direction [see Fig. 2(c)]. Out-of-plane flyout of the two parachutes is ignored. The dumbbell is illustrated in Fig. 3. A rigid body B contains two particles. Particle P_C has a mass of m_C, the total mass of two parachutes, which includes dry mass as well as the mass of air trapped in each of the canopies. Particle P_L has a mass of m_L and represents the capsule. Body B moves such that P_C and P_L remain at all times in a plane fixed in a Newtonian reference frame N. A right-handed set of mutually perpendicular unit vectors $\hat{\mathbf{n}}_1$, $\hat{\mathbf{n}}_2$, and $\hat{\mathbf{n}}_3$ is fixed in N. Unit vectors $\hat{\mathbf{n}}_1$ and $\hat{\mathbf{n}}_3$ lie in the plane in which motion takes place, and are directed as shown in Fig. 3; $\hat{\mathbf{n}}_1$ is horizontal, $\hat{\mathbf{n}}_2$ is directed into the page, and $\hat{\mathbf{n}}_3$ is vertical, directed downward. A right-handed set of mutually perpendicular unit vectors $\hat{\mathbf{b}}_1$, $\hat{\mathbf{b}}_2$, and $\hat{\mathbf{b}}_3$ is fixed in B. Unit vectors $\hat{\mathbf{b}}_1$ and $\hat{\mathbf{b}}_3$ are directed as shown in Fig. 3; $\hat{\mathbf{b}}_1$ has the same direction as the position vector $\mathbf{r}^{P_C P_L}$ from P_C to P_L. Unit vector $\hat{\mathbf{b}}_2$ is directed into the page; note that it is fixed in N as well as in B. Unit vectors $\hat{\mathbf{n}}_1$, $\hat{\mathbf{n}}_2$, $\hat{\mathbf{n}}_3$ are related to $\hat{\mathbf{b}}_1$, $\hat{\mathbf{b}}_2$, $\hat{\mathbf{b}}_3$ as indicated in Table 1. The entry in the rth row and sth column (not counting the row or the column containing unit vectors) is the dot product $\hat{\mathbf{n}}_r \cdot \hat{\mathbf{b}}_s$ $(r, s = 1, 2, 3)$.

B. Kinematics

Let ${}^N\boldsymbol{\omega}^B$ denote the angular velocity of B in N, and let ${}^N\boldsymbol{\alpha}^B$ represent the angular acceleration of B in N.

$$ {}^N\boldsymbol{\omega}^B = \dot{\theta}\,\hat{\mathbf{b}}_2 \tag{1} $$

$$ {}^N\boldsymbol{\alpha}^B = \ddot{\theta}\,\hat{\mathbf{b}}_2 \tag{2} $$

Table 1. Direction Cosines.

	$\hat{\mathbf{b}}_1$	$\hat{\mathbf{b}}_2$	$\hat{\mathbf{b}}_3$
$\hat{\mathbf{n}}_1$	$\sin\theta$	0	$-\cos\theta$
$\hat{\mathbf{n}}_2$	0	1	0
$\hat{\mathbf{n}}_3$	$\cos\theta$	0	$\sin\theta$

The mass center of B, $B^\star$, is fixed in B between particles P_C and P_L. The distance R_L from $B^\star$ to P_L can be expressed in terms of the distance L between P_C and P_L.

$$R_L = \frac{m_C}{m_C + m_L} L \tag{3}$$

The distance R_C from $B^\star$ to P_C can be expressed similarly,

$$R_C = \frac{m_L}{m_C + m_L} L \tag{4}$$

The velocity of $B^\star$ in N is denoted by ${}^N\mathbf{v}^{B^\star}$. Because P_C, P_L, and $B^\star$ are all fixed in B, the theorem for the velocities of two points fixed in a rigid body can be used to obtain the velocities in N of P_C and P_L in terms of ${}^N\mathbf{v}^{B^\star}$.

$${}^N\mathbf{v}^{P_C} = {}^N\mathbf{v}^{B^\star} + {}^N\boldsymbol{\omega}^{B} \times \mathbf{r}^{B^\star P_C} = {}^N\mathbf{v}^{B^\star} + R_C\dot{\theta}\,\hat{\mathbf{b}}_3 \tag{5}$$

$${}^N\mathbf{v}^{P_L} = {}^N\mathbf{v}^{B^\star} + {}^N\boldsymbol{\omega}^{B} \times \mathbf{r}^{B^\star P_L} = {}^N\mathbf{v}^{B^\star} - R_L\dot{\theta}\,\hat{\mathbf{b}}_3 \tag{6}$$

where the position vectors are given by $\mathbf{r}^{B^\star P_C} = -R_C\hat{\mathbf{b}}_1$ and $\mathbf{r}^{B^\star P_L} = R_L\hat{\mathbf{b}}_1$. Likewise, the theorem for the accelerations of two points fixed in a rigid body allows one to write the accelerations in N of P_C and P_L in terms of ${}^N\mathbf{a}^{B^\star}$, the acceleration of $B^\star$ in N.

$${}^N\mathbf{a}^{P_C} = {}^N\mathbf{a}^{B^\star} + {}^N\boldsymbol{\alpha}^{B} \times \mathbf{r}^{B^\star P_C} + {}^N\boldsymbol{\omega}^{B} \times {}^N\boldsymbol{\omega}^{B} \times \mathbf{r}^{B^\star P_C} = {}^N\mathbf{a}^{B^\star} + R_C(\ddot{\theta}\,\hat{\mathbf{b}}_3 + \dot{\theta}^2\,\hat{\mathbf{b}}_1) \tag{7}$$

$${}^N\mathbf{a}^{P_L} = {}^N\mathbf{a}^{B^\star} + {}^N\boldsymbol{\alpha}^{B} \times \mathbf{r}^{B^\star P_L} + {}^N\boldsymbol{\omega}^{B} \times {}^N\boldsymbol{\omega}^{B} \times \mathbf{r}^{B^\star P_L} = {}^N\mathbf{a}^{B^\star} - R_L(\ddot{\theta}\,\hat{\mathbf{b}}_3 + \dot{\theta}^2\,\hat{\mathbf{b}}_1) \tag{8}$$

C. Forces Acting on P_C and P_L

The resultant of the forces acting on P_L is given by

$$\mathbf{F}_L = W_L\hat{\mathbf{n}}_3 - T\hat{\mathbf{b}}_1 \tag{9}$$

where $-T\hat{\mathbf{b}}_1$ represents the internal force applied to P_L in order to keep it fixed in rigid body B, $W_L = m_L\,g$, and g is the magnitude of the local gravitational force per unit of mass. As mentioned earlier, aerodynamic force acting on the capsule is neglected. The resultant of the forces acting on P_C is given by

$$\mathbf{F}_C = W_C\hat{\mathbf{n}}_3 + (T - A_x)\hat{\mathbf{b}}_1 + A_z\hat{\mathbf{b}}_3 \tag{10}$$

where A_x and A_z characterize the resultant of the aerodynamic forces applied to the two parachutes represented by P_C. W_C is the sum of dry weights of the two parachutes; the weight of the air trapped in their canopies is ignored because the gravitational force exerted on that air is assumed to be counteracted by buoyancy effects from the ambient atmosphere.

D. Dynamics

B has three degrees of freedom in N, each of which is associated with a dynamical equation of motion. Two equations of motion can be obtained from the vector equation that governs translation of $B^\star$,

$$\mathbf{F}_C + \mathbf{F}_L = (m_C + m_L)\,{}^N\mathbf{a}^{B^\star} \tag{11}$$

${}^N\mathbf{a}^{B^\star}$ can be expressed either in terms of $\hat{\mathbf{b}}_1$ and $\hat{\mathbf{b}}_3$, or in terms of $\hat{\mathbf{n}}_1$ and $\hat{\mathbf{n}}_3$. In the first case,

$$ {}^N\mathbf{a}^{B^\star} = \frac{1}{m_C + m_L}\left\{[(W_C + W_L)\cos\theta - A_x]\,\hat{\mathbf{b}}_1 + [(W_C + W_L)\sin\theta + A_z]\,\hat{\mathbf{b}}_3\right\} \tag{12}$$

This expression for ${}^N\mathbf{a}^{B^\star}$ can be used together with Eqs. (7) and (8) to obtain expressions for the accelerations in N of P_C and P_L, respectively, in terms of $\hat{\mathbf{b}}_1$ and $\hat{\mathbf{b}}_3$. Alternatively, ${}^N\mathbf{a}^{B^\star}$ can be written as

$$ {}^N\mathbf{a}^{B^\star} = \frac{1}{m_C + m_L}\left\{-[A_x\sin\theta + A_z\cos\theta]\,\hat{\mathbf{n}}_1 + [W_C + W_L - A_x\cos\theta + A_z\sin\theta]\,\hat{\mathbf{n}}_3\right\} \tag{13}$$

The quantities ${}^N\mathbf{a}^{B^\star}\cdot\hat{\mathbf{n}}_1$ and ${}^N\mathbf{a}^{B^\star}\cdot\hat{\mathbf{n}}_3$ can be integrated with respect to time to obtain ${}^N\mathbf{v}^{B^\star}\cdot\hat{\mathbf{n}}_1$ and ${}^N\mathbf{v}^{B^\star}\cdot\hat{\mathbf{n}}_3$, respectively, and these in turn can be integrated to obtain horizontal and vertical displacements of $B^\star$.

In this paper we are especially interested in the third equation of motion, which governs θ. According to Kane's method (Ref. [8]),

$$ R_C\hat{\mathbf{b}}_3\cdot(\mathbf{F}_C - m_C\,{}^N\mathbf{a}^{P_C}) - R_L\hat{\mathbf{b}}_3\cdot(\mathbf{F}_L - m_L\,{}^N\mathbf{a}^{P_L}) = 0 \tag{14}$$

where $R_C\hat{\mathbf{b}}_3$ and $-R_L\hat{\mathbf{b}}_3$ are the vector coefficients of $\dot\theta$ in the expressions for ${}^N\mathbf{v}^{P_C}$ and ${}^N\mathbf{v}^{P_L}$, respectively [see Eqs. (5) and (6)]. After carrying out the required dot products and keeping in mind that $m_C R_C = m_L R_L$, one obtains

$$ (m_C {R_C}^2 + m_L {R_L}^2)\ddot\theta = R_C(W_C\sin\theta + A_z) - R_L W_L\sin\theta \tag{15}$$

One can also obtain this result by writing Euler's equation of rotational motion for B; the coefficient multiplying $\ddot\theta$ is the central moment of inertia of B for a line parallel to $\hat{\mathbf{b}}_2$. In view of Eqs. (3) and (4) and the fact that $W_L = m_L\,g$, Eq. (15) can be rewritten as

$$ \ddot\theta + \frac{1}{m_C L}[(m_C\,g - W_C)\sin\theta - A_z] = 0 \tag{16}$$

E. Aerodynamics

A_x, the magnitude of the resultant of the aerodynamic axial forces applied to the two parachutes, can be expressed as

$$ A_x = 2q_\infty S_{\text{ref}} C_A \tag{17}$$

where q_∞ is the dynamic pressure, S_{ref} is the reference area of a single parachute, and C_A is the drag coefficient for a single parachute. The absolute value of A_z is the magnitude of the resultant of the aerodynamic normal forces applied to the two parachutes; A_z can be expressed as

$$ A_z = -2q_\infty S_{\text{ref}} C_N \tag{18}$$

C_N is the aerodynamic normal force coefficient for a single parachute. In a steady-state flight condition, C_A and C_N are nonlinear functions of α, the instantaneous angle of attack of the parachute, as shown with the solid curves in Fig. 1 and discussed in Ref. [2]. Equilibria exist at the three points where $C_N = 0$. The equilibrium point $\alpha = 0$ is unstable, and the two equilibrium points at $\alpha = \pm\alpha_0$ are stable, where $\alpha_0 = 20$ deg in Fig. 1. In our analysis we treat C_A as constant and take C_{N_α}, the slope of the curve for C_N indicated with the black line in Fig. 1, to be constant in the neighborhood of an equilibrium point. C_N is expressed as

$$ C_N = C_{N_\alpha}(\alpha - \alpha_0) + C_{N_{\dot\alpha}}\dot\alpha_Q = C_{N_\alpha}(\alpha - \alpha_0) + C_{N_{\dot\alpha}}\dot\theta \tag{19}$$

where α_0 is the trimmed angle of attack of the parachute, and the term $C_{N_{\dot\alpha}}\dot\alpha_Q$ is added to account for unsteady flow when α is changing with time. In the literature (for example, Refs. [9] and [10]), $C_{N_{\dot\alpha}}$ is multiplied by the time derivative of the angle of attack at the aircraft mass center, a point having a steady-state velocity. Instead, we use the time derivative of angle of attack at a point Q because, as discussed presently, the velocity of this point is nearly constant. As indicated in Fig. 2(c), $\alpha_Q = \theta - \gamma$; therefore, $\dot\alpha_Q = \dot\theta$ because γ is constant.

As will be discussed in detail in Sec. III.G, one can determine the location of a pivot point Q whose velocity ${}^N\mathbf{v}^Q$ in N is nearly constant. The magnitude of ${}^N\mathbf{v}^Q$ is denoted by V_∞ and regarded as constant. Hence, ${}^N\mathbf{v}^Q$ can be written as

$$ {}^N\mathbf{v}^Q = V_\infty(\cos\alpha_Q\,\hat{\mathbf{b}}_1 + \sin\alpha_Q\,\hat{\mathbf{b}}_3) \tag{20}$$

where α_Q is the angle of attack at Q (see Fig. 2). The velocity ${}^N\mathbf{v}^{P_C}$ of P_C in N can then be expressed as

$$ {}^N\mathbf{v}^{P_C} = {}^N\mathbf{v}^Q + L_C\dot{\theta}\,\hat{\mathbf{b}}_3 = V_\infty\cos\alpha_Q\,\hat{\mathbf{b}}_1 + (V_\infty\sin\alpha_Q + L_C\dot{\theta})\hat{\mathbf{b}}_3 \tag{21}$$

where $\mathbf{r}^{QP_C} = -L_C\hat{\mathbf{b}}_1$ is the position vector from Q to P_C. The tangent of the angle of attack α at P_C is given by

$$ \tan\alpha = \frac{{}^N\mathbf{v}^{P_C}\cdot\hat{\mathbf{b}}_3}{{}^N\mathbf{v}^{P_C}\cdot\hat{\mathbf{b}}_1} = \frac{V_\infty\sin\alpha_Q + L_C\dot{\theta}}{V_\infty\cos\alpha_Q} \tag{22}$$

When both angles of attack are small, the following approximation can be used.

$$ \alpha \approx \alpha_Q + \frac{L_C\dot{\theta}}{V_\infty} \tag{23}$$

The second term on the right-hand side is referred to as angle of attack induced by $\dot{\theta}$. According to Fig. 2(c), $\alpha_Q = \theta - \gamma = \theta + \alpha_0$, where $\alpha_0 = -\gamma$ is constant. Thus,

$$ \alpha - \alpha_0 \approx \theta + \frac{L_C\dot{\theta}}{V_\infty} \tag{24}$$

Substitution from Eq. (24) into Eq. (19) yields

$$\begin{aligned} C_N &= C_{N_\alpha}\left(\theta + \frac{L_C\dot{\theta}}{V_\infty}\right) + C_{N_{\dot{\alpha}}}\dot{\theta} \\ &= C_{N_\alpha}\theta + \left(C_{N_{\dot{\alpha}}} + C_{N_\alpha}\frac{L_C}{V_\infty}\right)\dot{\theta} \\ &\triangleq C_{N_\alpha}\theta + (C_{N_{\dot{\alpha}}})_{\text{tot}}\,\dot{\theta} \end{aligned} \tag{25}$$

where $(C_{N_{\dot{\alpha}}})_{\text{tot}}$, total aerodynamic damping, is defined to be $C_{N_{\dot{\alpha}}} + C_{N_\alpha}L_C/V_\infty$. The units of C_{N_α} and $C_{N_{\dot{\alpha}}}$ are henceforth taken to be rad^{-1} and s/rad, respectively. Consequently, the units of θ and $\dot{\theta}$ are taken to be rad and rad/s.

Substitution from Eq. (25) into (18) and then into (16) yields

$$ A_z = -2q_\infty S_{\text{ref}}\left[(C_{N_{\dot{\alpha}}})_{\text{tot}}\,\dot{\theta} + C_{N_\alpha}\theta\right] \tag{26}$$

and

$$ \ddot{\theta} + \frac{2q_\infty S_{\text{ref}}}{m_C L}(C_{N_{\dot{\alpha}}})_{\text{tot}}\,\dot{\theta} + \frac{1}{m_C L}\left[(m_C\,g - W_C)\sin\theta + 2q_\infty S_{\text{ref}}C_{N_\alpha}\theta\right] = 0 \tag{27}$$

The total weight of the system, W_{tot}, is equal to the sum of the weight of the load and the dry weight of the two parachutes. In other words, $W_{\text{tot}} = W_L + W_C$. During equilibrium descent in the plane depicted in Fig. 2(b), the resultant axial force applied to the two parachutes balances the gravitational force $W_{\text{tot}}\hat{\mathbf{n}}_3$, resulting in zero acceleration in the vertical direction. Consequently, W_{tot} is equal to A_x, or $W_{\text{tot}} = A_x = 2q_\infty S_{\text{ref}}C_A$. Thus, $2q_\infty S_{\text{ref}}$ can be replaced with W_{tot}/C_A, and Eq. (27) can be rewritten as

$$ \ddot{\theta} + \frac{W_{\text{tot}}}{m_C L C_A}(C_{N_{\dot{\alpha}}})_{\text{tot}}\,\dot{\theta} + \frac{1}{m_C L}\left[(m_C\,g - W_C)\sin\theta + \frac{W_{\text{tot}}}{C_A}C_{N_\alpha}\theta\right] = 0 \tag{28}$$

F. Equation of Motion for Small Angles

When θ remains small, Eq. (28) can be approximated as

$$\ddot{\theta} + \frac{W_{\text{tot}}}{m_C L C_A}(C_{N_{\dot{\alpha}}})_{\text{tot}}\,\dot{\theta} + \frac{1}{m_C L}\left[(m_C\,g - W_C) + \frac{W_{\text{tot}}}{C_A}C_{N_\alpha}\right]\theta = 0 \tag{29}$$

This second-order linear differential equation has the form

$$\ddot{x} + 2b\dot{x} + {\omega_n}^2 x = 0 \tag{30}$$

which governs damped free vibrations. ω_n is referred to as the circular natural frequency, and b/ω_n is the fraction of critical damping, or damping ratio. We define b and ${\omega_n}^2$ as

$$b \triangleq \frac{W_{\text{tot}}}{2m_C L C_A}(C_{N_{\dot{\alpha}}})_{\text{tot}} \tag{31}$$

and

$${\omega_n}^2 \triangleq \frac{1}{m_C L}\left[(m_C\,g - W_C) + \frac{W_{\text{tot}}}{C_A}C_{N_\alpha}\right] \tag{32}$$

The general solution of Eq. (29) is then given by

$$\theta = e^{-bt}\left[C_1 \sin(\omega_d\,t) + C_2 \cos(\omega_d\,t)\right] \tag{33}$$

where the damped natural frequency, ω_d, is given by

$$\omega_d = \sqrt{{\omega_n}^2 - b^2} \tag{34}$$

and the constants C_1 and C_2 can be expressed in terms of the initial values $\theta_0 = \theta(t=0)$ and $\dot{\theta}_0 = \dot{\theta}(t=0)$,

$$C_1 = \frac{1}{\omega_d}\left(\dot{\theta}_0 + b\theta_0\right) \tag{35}$$

$$C_2 = \theta_0 \tag{36}$$

The constants appearing in the fraction on the right-hand side of Eq. (31) are all positive; therefore, the sign of b is determined by the sign of $(C_{N_{\dot{\alpha}}})_{\text{tot}}$. Exponential decay in θ occurs for $(C_{N_{\dot{\alpha}}})_{\text{tot}} > 0$, whereas there is exponential growth in θ for $(C_{N_{\dot{\alpha}}})_{\text{tot}} < 0$. In either case, the damped frequency ω_d of oscillations in θ is smaller than ω_n; consequently, the period of damped oscillations is larger than that of undamped oscillations.

G. Pivot Point

Solutions of dynamical equations governing planar motions of the dumbbell reveal the existence of a point Q, on the line joining P_L and P_C, whose trajectory in N is very nearly a straight line; from this observation, it can be inferred that the magnitude of the acceleration ${}^N\mathbf{a}^Q$ of Q in N is nearly zero. In what follows, we find the distance L_L from P_L to Q such that ${}^N\mathbf{a}^Q \cdot \hat{\mathbf{b}}_3 = 0$ for undamped oscillations having small amplitude. It is also shown that, under the same conditions, ${}^N\mathbf{a}^Q \cdot \hat{\mathbf{b}}_1$ is small when the initial values θ_0 and $\dot{\theta}_0$ are zero and small, respectively. Q is referred to as the pivot point; the smaller the value of L_L is, the better the landing conditions will be for the capsule.

The acceleration ${}^N\mathbf{a}^Q$ of Q in N is, with the aid of Eq. (12), given by

$$\begin{aligned} {}^N\mathbf{a}^Q &= {}^N\mathbf{a}^{B^*} + (L_L - R_L)(\ddot{\theta}\,\hat{\mathbf{b}}_3 + \dot{\theta}^2\,\hat{\mathbf{b}}_1) \\ &= \left[\frac{(W_C + W_L)\cos\theta - A_x}{m_C + m_L} + (L_L - R_L)\dot{\theta}^2\right]\hat{\mathbf{b}}_1 + \left[\frac{(W_C + W_L)\sin\theta + A_z}{m_C + m_L} + (L_L - R_L)\ddot{\theta}\right]\hat{\mathbf{b}}_3 \end{aligned} \tag{37}$$

One can determine the value of L_L such that ${}^N\mathbf{a}^Q \cdot \hat{\mathbf{b}}_3 = 0$ when θ remains small and oscillations are undamped. Substitution from Eq. (3) leads to

$${}^N\mathbf{a}^Q \cdot \hat{\mathbf{b}}_3 = \frac{(W_C + W_L)\sin\theta + A_z - m_C L\ddot{\theta}}{m_C + m_L} + L_L\ddot{\theta} = 0 \tag{38}$$

In view of Eq. (16) and the fact that $W_L = m_L\, g$, we have

$$\frac{(W_C + W_L)\sin\theta + (m_C\, g - W_C)\sin\theta}{m_C + m_L} + L_L\ddot{\theta} = g\sin\theta + L_L\ddot{\theta} = 0 \tag{39}$$

Thus, after substitution from Eq. (28) with $(C_{N_\alpha^\star})_{\rm tot} = 0$,

$$-\,L_L\ddot{\theta} = \frac{L_L}{m_C L}\left[(m_C\, g - W_C)\sin\theta + \frac{W_{\rm tot}}{C_A}C_{N_\alpha}\theta\right] = g\sin\theta \tag{40}$$

When θ remains small, L_L can be expressed as

$$L_L = \frac{m_C\, g\, C_A}{(m_C\, g - W_C)\, C_A + W_{\rm tot}C_{N_\alpha}}\, L \tag{41}$$

It is easily shown that $L_L = R_L$ when $C_A = C_{N_\alpha}$, in which case Q is coincident with $B^\star$. When $C_{N_\alpha} = 0$, it is evident that L_L slightly exceeds L because the numerator in Eq. (41) becomes the sum of the masses of the dry parachutes and entrapped air, whereas the denominator consists only of the masses of entrapped air.

Now, ${}^N\mathbf{a}^Q \cdot \hat{\mathbf{b}}_1$ is given by

$${}^N\mathbf{a}^Q \cdot \hat{\mathbf{b}}_1 = \frac{(W_C + W_L)\cos\theta - A_x}{m_C + m_L} + (L_L - R_L)\dot{\theta}^2 \tag{42}$$

As discussed prior to Eq. (28), the resultant aerodynamic axial force A_x applied to P_C is equal to $W_{\rm tot}$ in equilibrium descent. Hence, in view of Eq. (12), the first term on the right-hand side of Eq. (42),

$${}^N\mathbf{a}^{B^\star} \cdot \hat{\mathbf{b}}_1 = \frac{(W_C + W_L)\cos\theta - A_x}{m_C + m_L} = \frac{W_{\rm tot}(\cos\theta - 1)}{m_C + m_L} \tag{43}$$

is small when θ remains small. The time derivative of θ can be obtained from Eq. (33).

$$\dot{\theta} = -b\theta + \omega_d\, e^{-bt}\left[C_1\cos(\omega_d\, t) - C_2\sin(\omega_d\, t)\right] \tag{44}$$

For undamped oscillations $(C_{N_\alpha^\star})_{\rm tot} = 0$ and $b = 0$, and this relationship is simplified to

$$\dot{\theta} = \omega_n\left[C_1\cos(\omega_n\, t) - C_2\sin(\omega_n\, t)\right] \tag{45}$$

When the initial value θ_0 vanishes, $\dot{\theta}^2$ is given by

$$\dot{\theta}^2 = [\dot{\theta}_0\, \cos(\omega_n\, t)]^2 \tag{46}$$

Thus, when $\dot{\theta}_0$ is small (less than 1 rad/s), $\dot{\theta}^2$ is smaller still.

In the foregoing circumstances, then, ${}^N\mathbf{a}^Q \cdot \hat{\mathbf{b}}_1$ is small, as is the magnitude of ${}^N\mathbf{a}^Q$, in which case Q travels in nearly a straight line and has velocity in N that is nearly constant. This is illustrated in Sec. IV with time histories of the dot products of $\hat{\mathbf{b}}_1$ and $\hat{\mathbf{b}}_3$ with the accelerations in N of Q, the mass center $B^\star$, the capsule particle P_L, and the parachute particle P_C. Time histories of the magnitude of the accelerations of these four points, as well as trajectories of Q, P_L, and P_C, are also presented.

As the distance L_L decreases the pivot point becomes closer to the capsule, which decreases the distance the payload travels over a circular path during pendulum motion. Equation (41) is a key relationship for a two-parachute system that substantiates observations made in previous studies of pendulum motion: 1) increasing the parachute C_{N_α} moves the pivot point towards the payload, and reduces the distance traveled by the capsule as it swings. 2) decreasing the parachute drag coefficient (by increasing its porosity) moves the pivot point towards the payload, and reduces the distance traveled by the capsule as it swings; however, this benefit comes at the expense of increasing the steady-state descent rate, which may not be desirable. 3) decreasing the payload mass (the largest contributor to $W_{\rm tot}$) shifts the pivot point towards the parachutes, and increases the distance traveled by the capsule as it swings. 4) an increase in the atmospheric density increases the mass of the air entrapped in the canopy (the larger part of m_C) and moves the pivot point towards the parachutes. These observations are consistent with conclusions drawn in Refs. [2], [5], and [6].

IV. Numerical Results

Numerical results are now presented for two purposes. First, we use translational equations of motion for the dumbbell and the closed-form solution for rotational motion, Eq. (33), to demonstrate that the acceleration of Q in N is nearly zero and Q travels essentially in a straight line, as discussed in Sec. III. This is accomplished by determining time histories of the accelerations in N of $B^\star$, Q, P_C, and P_L for several values of C_A, C_{N_α}, and $(C_{N_{\dot\alpha}})_{\rm tot}$. Comparisons are made of dot products of the accelerations with $\hat{\mathbf{b}}_1$ and $\hat{\mathbf{b}}_3$, and of the magnitudes of the accelerations. Trajectories of Q, P_C, and P_L are also illustrated. The second purpose is to examine the horizontal and vertical projections of the velocities in N of P_C and P_L for several values of C_A and C_{N_α}. Results obtained with the dumbbell model are compared with results obtained from numerical simulations based on more sophisticated models of the capsule and parachutes.

System parameters used to produce the numerical results are recorded in Table 2.

Table 2. System Parameters.

parameter	value	units
$S_{\rm ref}$ (single parachute)	10563	$\rm ft^2$
C_A (single parachute)	0.85	-
L	235	ft
Capsule Weight, W_L	20814	$\rm lb_f$
Dry Weight of Two Parachutes, W_C	656	$\rm lb_f$
Total Mass of Two Parachutes, (dry and entrapped air), m_C	614	slugs
Distance from System Center of Mass to Capsule CM, R_L	114.43	ft

A. Acceleration of Pivot Point

The behavior of pivot point Q, discussed in Sec. III.G, is illustrated for various values of aerodynamic coefficients. Figures 4 – 10 show results for cases a–e, each of which is associated with the parameters appearing in the corresponding row of Table 3. Values of L_L are obtained with Eq. (41) and entries in Table 2.

Table 3. Aerodynamic Parameters for Cases a–f.

case	C_A	C_{N_α} (1/rad)	L_L (ft)	$(C_{N_{\dot\alpha}})_{\rm tot}$ (s/rad)	q_∞ ($\rm lb_f/ft^2$)
a	0.85	0.85	114.43	0	1.190
b	0.85	0.30	174.02	0	1.198
c	0.85	0.00	243.07	0	1.215
d	0.85	0.85	114.43	−0.160	1.190
e	0.85	0.85	114.43	0.304	1.190
f	0.425	0.30	135.52	0	2.391

The time histories of θ presented in Fig. 4 are obtained with Eq. (33) and initial values $\theta_0 = 0$ and $\dot\theta_0 = 0.0873$ rad/s. Oscillations in cases a, b, and c are undamped. Exponential growth and exponential decay are exhibited in cases d and e, respectively.

Plots of the dot products of ${}^N\mathbf{a}^{B^\star}$ with $\hat{\mathbf{b}}_1$ and $\hat{\mathbf{b}}_3$ shown in Fig. 5 are obtained from Eqs. (12), (17), (26), (33), and (44). In cases a, b, and c, it is worth noting that the amplitude of ${}^N\mathbf{a}^{B^\star}\cdot\hat{\mathbf{b}}_3$ grows significantly as C_{N_α} decreases.

Projections of ${}^N\mathbf{a}^{Q}$ onto $\hat{\mathbf{b}}_1$ and $\hat{\mathbf{b}}_3$ displayed in Fig. 6 are produced with the aid of Eqs. (37), (29), (33), and (44). In cases a, b, and c, ${}^N\mathbf{a}^{Q}\cdot\hat{\mathbf{b}}_3$ is essentially zero, as expected for undamped motion. A

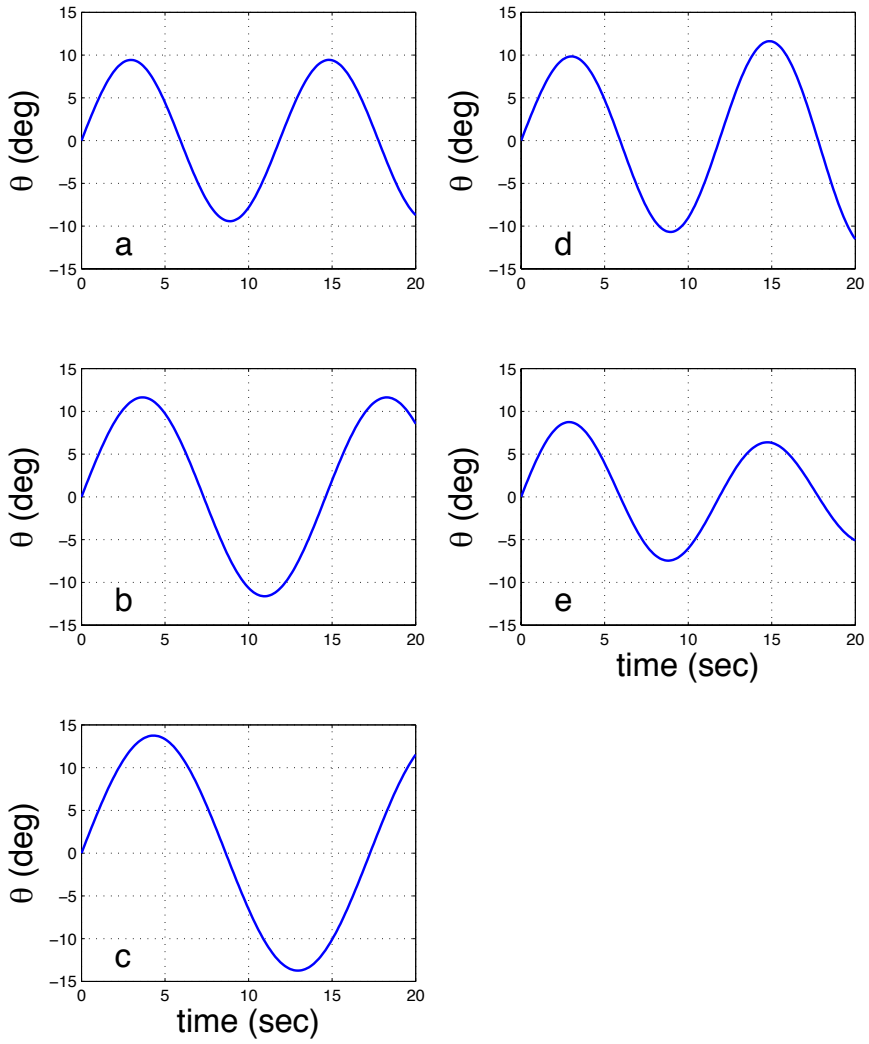

Figure 4. Swing Angle, Closed-form Solution, from Eq. (33).

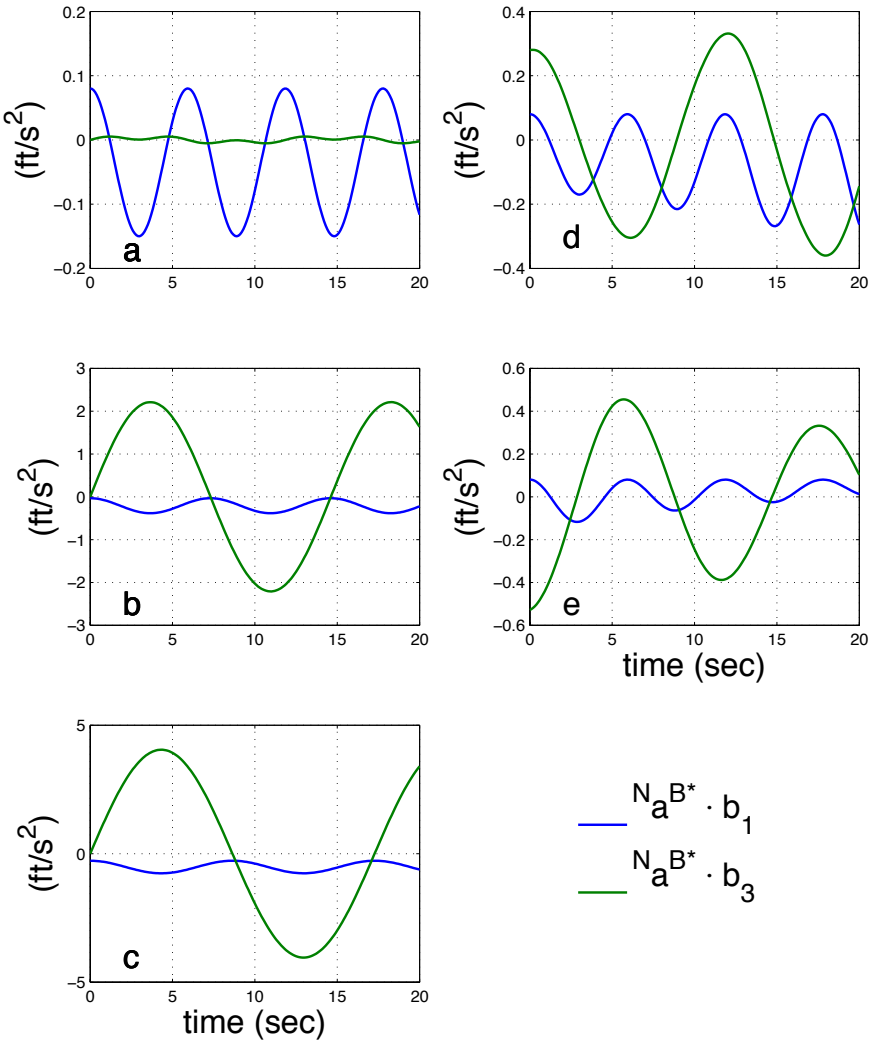

Figure 5. Acceleration of Mass Center in N, from Eq. (12).

comparison of cases a, d, and e here and in Fig. 5 indicate that ${}^N\mathbf{a}^Q = {}^N\mathbf{a}^{B^\star}$, which is consistent with Q being coincident with $B^\star$. As discussed in Sec. III.G, the two points are coincident when $C_A = C_{N_\alpha}$ because in that case $L_L = R_L$.

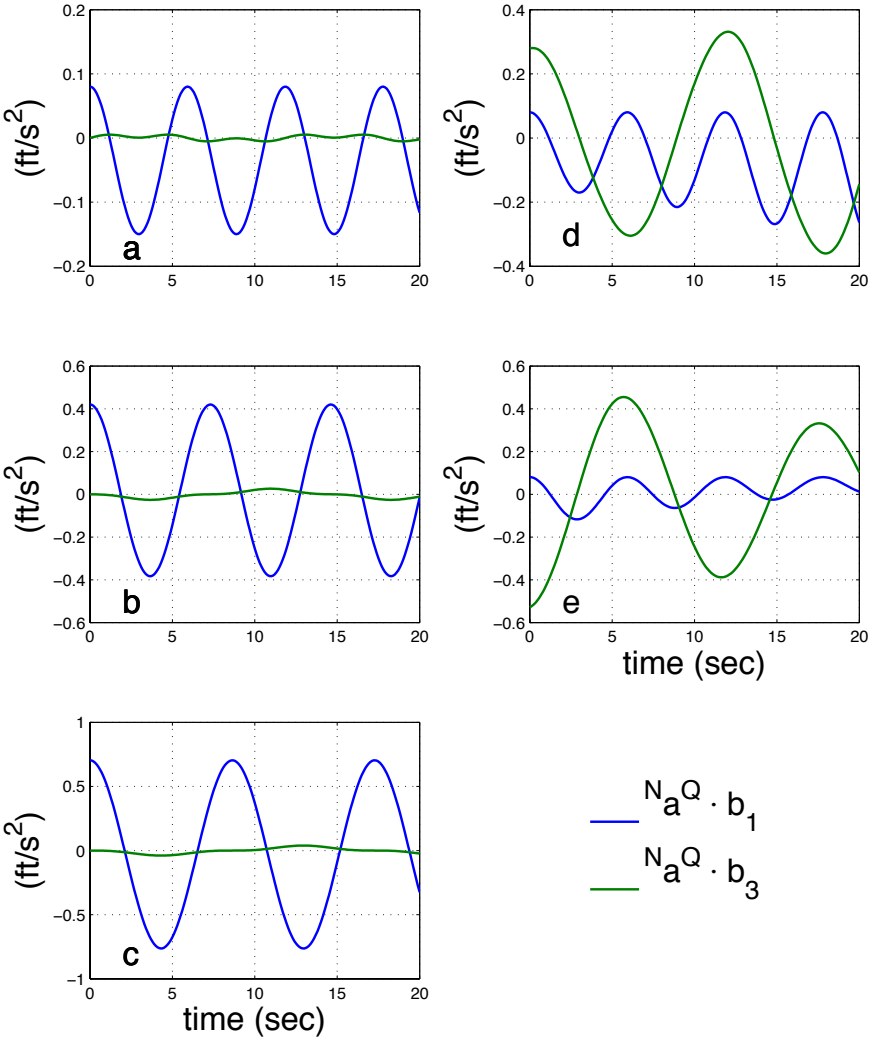

Figure 6. Acceleration of Pivot Point in N, from Eq. (37).

In Fig. 7 the time histories of ${}^N\mathbf{a}^{B^\star} \cdot \hat{\mathbf{b}}_1$ and ${}^N\mathbf{a}^Q \cdot \hat{\mathbf{b}}_1$ shown in Figs. 5 and 6 are compared with ${}^N\mathbf{a}^{P_C} \cdot \hat{\mathbf{b}}_1$ and ${}^N\mathbf{a}^{P_L} \cdot \hat{\mathbf{b}}_1$, which are formed using Eqs. (7), (8), (29), (33), and (44). In each case ${}^N\mathbf{a}^Q \cdot \hat{\mathbf{b}}_1$ is seen to be small, especially when compared to the curves in Fig. 8 for ${}^N\mathbf{a}^{B^\star} \cdot \hat{\mathbf{b}}_3$, ${}^N\mathbf{a}^{P_C} \cdot \hat{\mathbf{b}}_3$, and ${}^N\mathbf{a}^{P_L} \cdot \hat{\mathbf{b}}_3$.

In Fig. 8 the time histories of ${}^N\mathbf{a}^{B^\star} \cdot \hat{\mathbf{b}}_3$ and ${}^N\mathbf{a}^Q \cdot \hat{\mathbf{b}}_3$ shown in Figs. 5 and 6 are compared with ${}^N\mathbf{a}^{P_C} \cdot \hat{\mathbf{b}}_3$ and ${}^N\mathbf{a}^{P_L} \cdot \hat{\mathbf{b}}_3$, which are formed with the equations mentioned in connection with Fig. 7. In cases d and e, ${}^N\mathbf{a}^Q \cdot \hat{\mathbf{b}}_3$ has a small amplitude even when θ grows or decays exponentially. In cases a, b, and c, the amplitude of ${}^N\mathbf{a}^{P_L} \cdot \hat{\mathbf{b}}_3$ is increasing with L_L.

Time histories of the magnitudes of the accelerations in N of $B^\star$, Q, P_C, and P_L are displayed in Fig. 9. The magnitude of ${}^N\mathbf{a}^Q$ is small compared to those of the other points, which is an indication that Q travels nearly in a straight line. This is true for damped as well as the undamped motion. In cases a, b, and

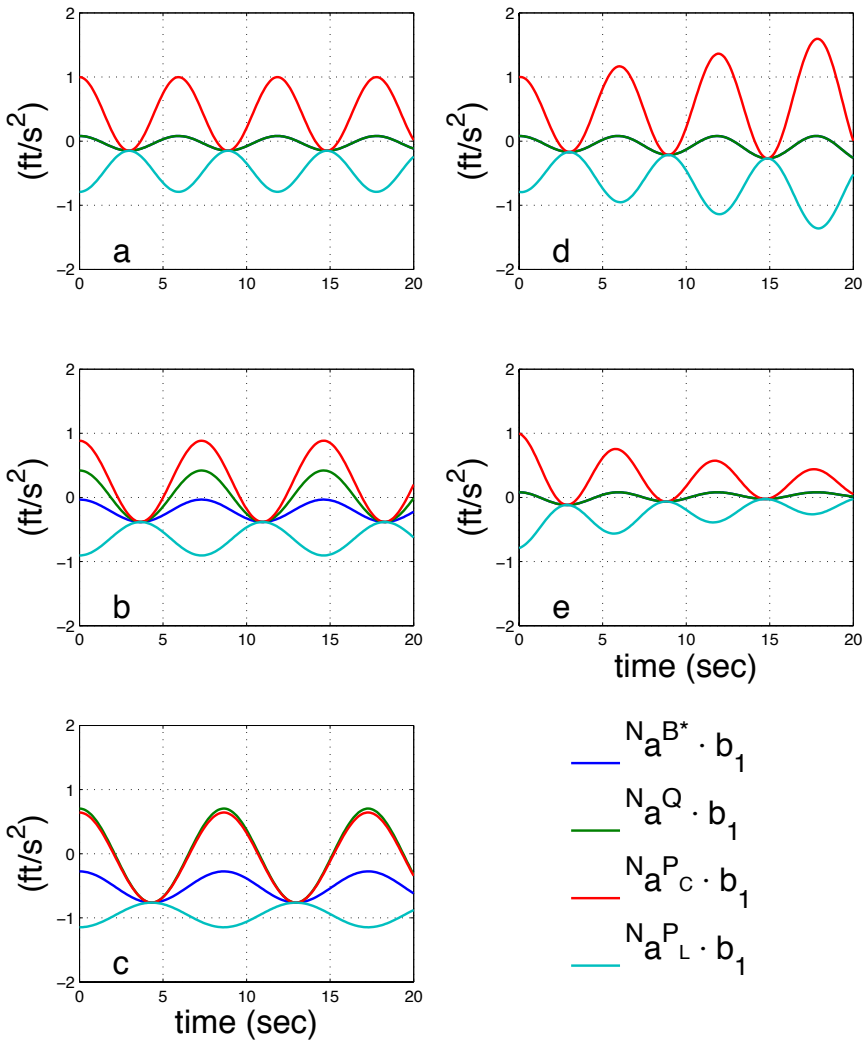

Figure 7. Acceleration in N of $B^\star$, Q, P_C, and P_L; Dot Product with $\hat{\mathbf{b}}_1$.

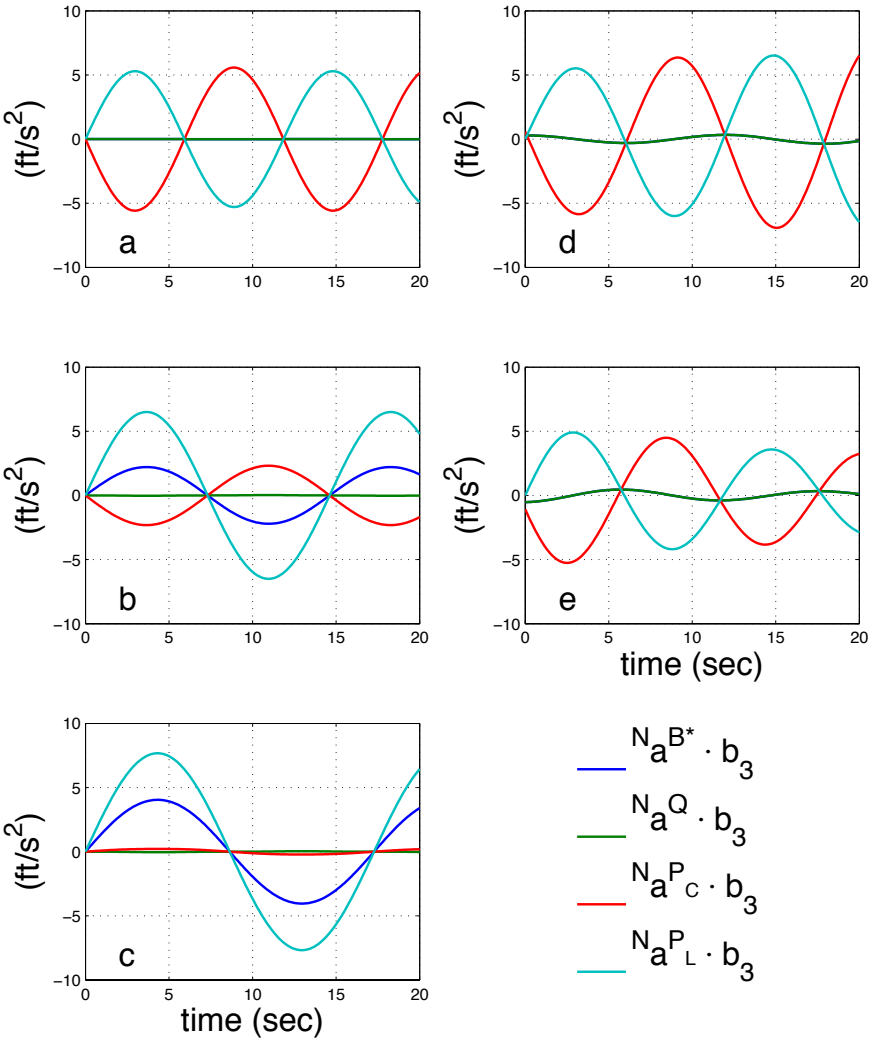

Figure 8. Acceleration in N of $B^\star$, Q, P_C, and P_L; Dot Product with $\hat{\mathbf{b}}_3$.

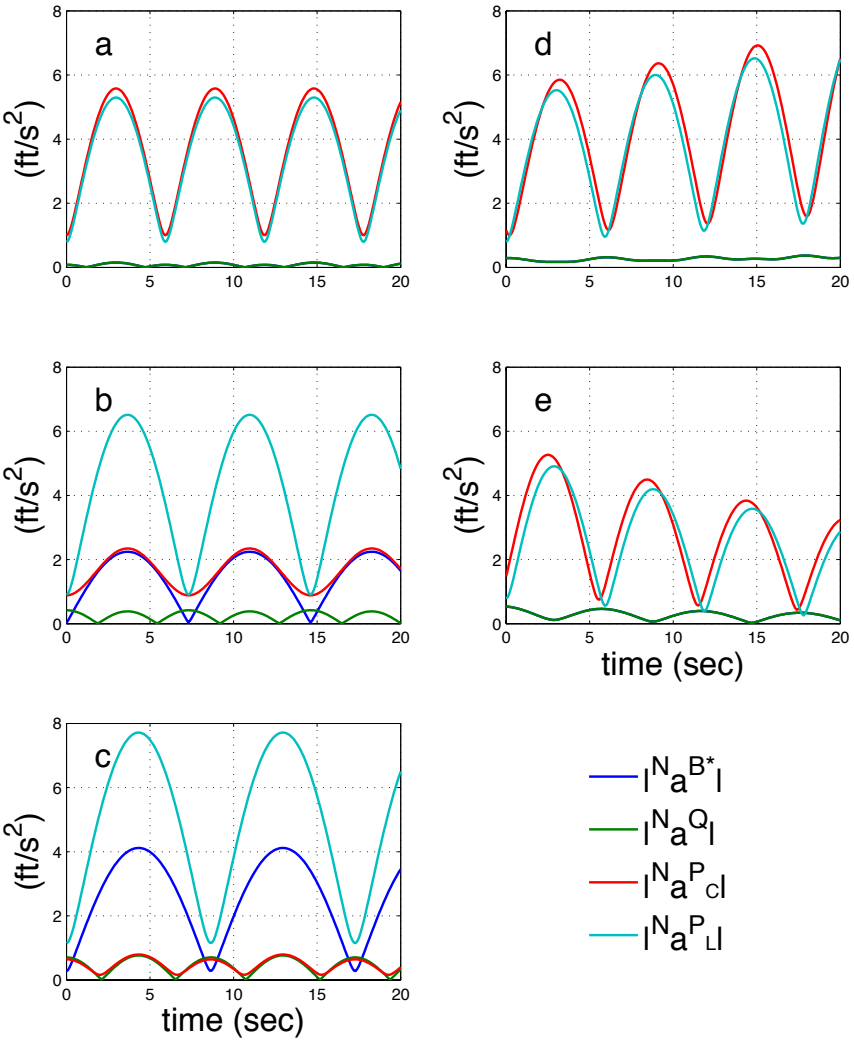

Figure 9. Magnitude of Acceleration in N of B^*, Q, P_C, and P_L.

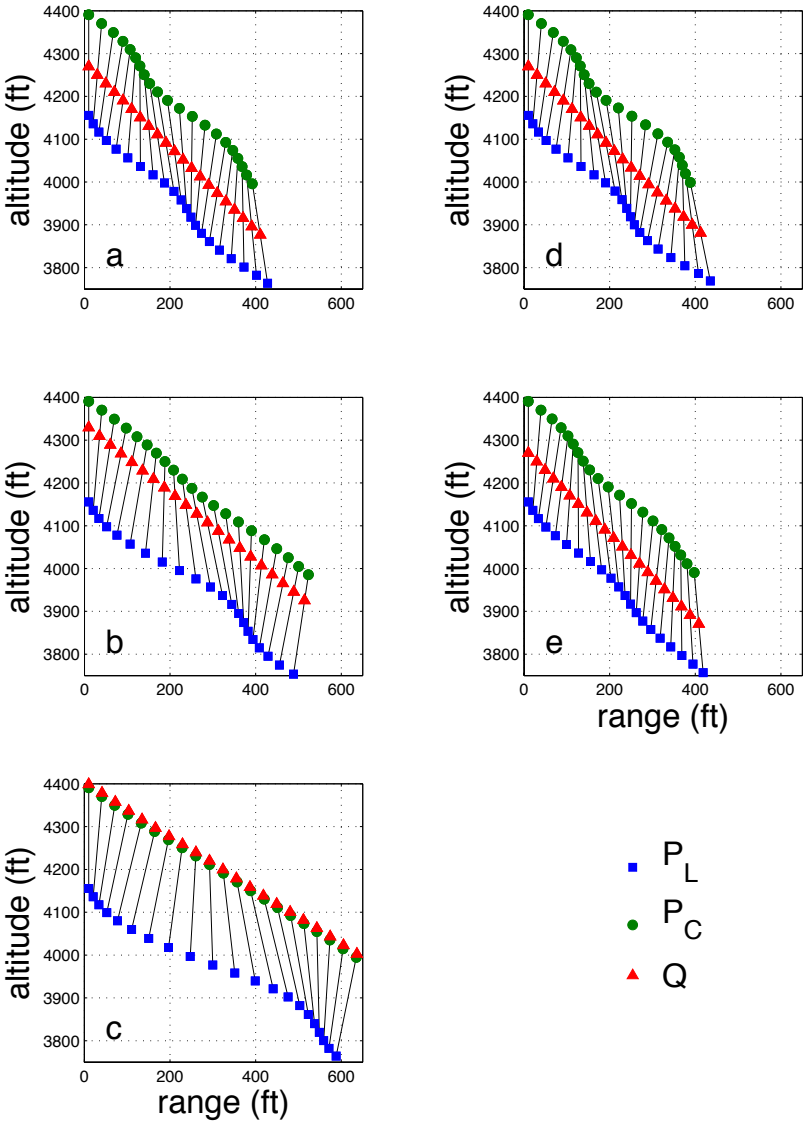

Figure 10. Trajectories in N of P_L, Q, and P_C.

c, the magnitude of the capsule's acceleration is increasing with L_L.

The trajectory in N of $B^\star$ can be obtained according to the discussion that follows Eq. (13), and then used together with a time history of θ to construct trajectories in N of P_L (blue square), Q (red triangle), and P_C (green circle), as shown in Fig. 10. The initial value of the mass center position is taken to be $\mathbf{r}^{OB^\star}(t=0) = -(10\hat{\mathbf{n}}_1 + 4270\hat{\mathbf{n}}_3)$ ft, where O is a point fixed in N at ground level, and the initial value of the velocity of the mass center in N is ${}^N\mathbf{v}^{B^\star}(t=0) = -20\hat{\mathbf{n}}_1 + 20\hat{\mathbf{n}}_3$ ft/s. The trajectory of the pivot point Q is seen to be nearly a straight line in each case.

B. Velocities of Capsule and Parachute

The horizontal and vertical speeds of the capsule and parachute are now examined in relation to the location of the pivot point. Results are obtained in three ways. First, three dynamical equations of motion for the dumbbell are numerically integrated; namely, Eq. (29) and two others that can be obtained from Eq. (13). Equations (5) and (6) also come into play. The second approach is to employ the CAPDYN simulation, whereas the third approach exercises the FAST simulation. Results obtained with the first, second, and third approaches are displayed with black, blue, and green curves, respectively, in Figs. 11 and 12.

CAPDYN (CAPsule DYNamics) is a software program that provides numerical solutions of equations governing the motion of a multi-degree-of-freedom system containing a capsule, and one or two parachutes. It was developed independently by the NASA Engineering and Safety Center as part of its investigation of pendulum dynamics.

FAST (Flight Analysis and Simulation Tool) is a multi-body, variable-degree-of-freedom simulation developed for the study of atmospheric and powered flight. It has been used extensively by the Capsule Parachute Assembly System project for pre-test analysis and post-test reconstruction, including modeling two-parachute cluster pendulum dynamics.

In both simulations the capsule can be treated as a particle, with three translational degrees of freedom in reference frame N, or as an extended rigid body with six degrees of freedom in N. Each parachute is regarded as a particle possessing three translational degrees of freedom relative to the capsule. Thus, the number of degrees of freedom in N possessed by the system ranges from six, when the capsule is treated as a particle connected to one parachute, to twelve, when the capsule is treated as a rigid body connected to two parachutes. In the simulations whose results are presented here, two parachutes are included in the model and the capsule is treated as a particle.

The flexible riser line that connects the capsule to a parachute is modeled as a massless spring and a damper. The line can exert a tensile force, but not a compressive force. When the capsule is treated as a rigid body, the point of attachment of the riser lines need not be coincident with the capsule's mass center. The capsule and parachutes are subject to gravitational and aerodynamic forces, in addition to the forces transmitted by the riser lines. In the case of a parachute, the gravitational force is calculated with the dry mass; the gravitational force exerted on the air trapped in the canopy is assumed to be counteracted by buoyancy effects from the ambient atmosphere. In applying Newton's second law, the acceleration in N of a parachute is scaled by the sum of the dry mass and the mass of the entrapped air.

Initial conditions and force models are chosen such that the system performs planar motion. The unit vectors $\hat{\mathbf{n}}_1$, $\hat{\mathbf{n}}_2$, and $\hat{\mathbf{n}}_3$ depicted in Fig. 3 correspond to west, north, and down, respectively, in CAPDYN and FAST simulations performed for present purposes. The simulations conducted for the purposes of this study involve no wind disturbance, no aerodynamic force applied to the capsule, and air density that does not vary with altitude. C_{N_α} and C_A are treated as constants.

The initial value of the mass center position is taken to be $\mathbf{r}^{OB^\star}(t=0) = -4500\hat{\mathbf{n}}_3$ ft. Initial values of the swing angle and its time derivative are $\theta_0 = 0$ and $\dot{\theta}_0 = 0.02$ rad/s. The initial velocity of $B^\star$ in N corresponds to a trim angle of attack of 10 deg. For cases a, b, and c, ${}^N\mathbf{v}^{B^\star}(t=0) = -5.94\hat{\mathbf{n}}_1 + 33.67\hat{\mathbf{n}}_3$ ft/s, whereas for case f, ${}^N\mathbf{v}^{B^\star}(t=0) = -8.3351\hat{\mathbf{n}}_1 + 47.27\hat{\mathbf{n}}_3$ ft/s.

According to Eq. (41), decreasing C_{N_α} moves the pivot point toward the parachute. This is reflected by increasing values of L_L in Table 3 for three cases of undamped oscillation, a, b, and c. Figures 4 and 10 show a decrease in C_{N_α} is accompanied by an increase in the amplitude of θ and in excursions of the capsule during pendulum motion. Figure 11 contains plots of $-{}^N\mathbf{v}^{P_L} \cdot \hat{\mathbf{n}}_1$ on the left side and $-{}^N\mathbf{v}^{P_C} \cdot \hat{\mathbf{n}}_1$ on the right side; these are the projections of the capsule and parachute velocities in the eastward direction. As can be seen, a decrease in C_{N_α} increases the amplitude of oscillations in the horizontal speed of the capsule, and decreases the amplitude of oscillations in the horizontal speed of the parachute. The results obtained from the dumbbell model are in very good agreement with those obtained from CAPDYN and FAST.

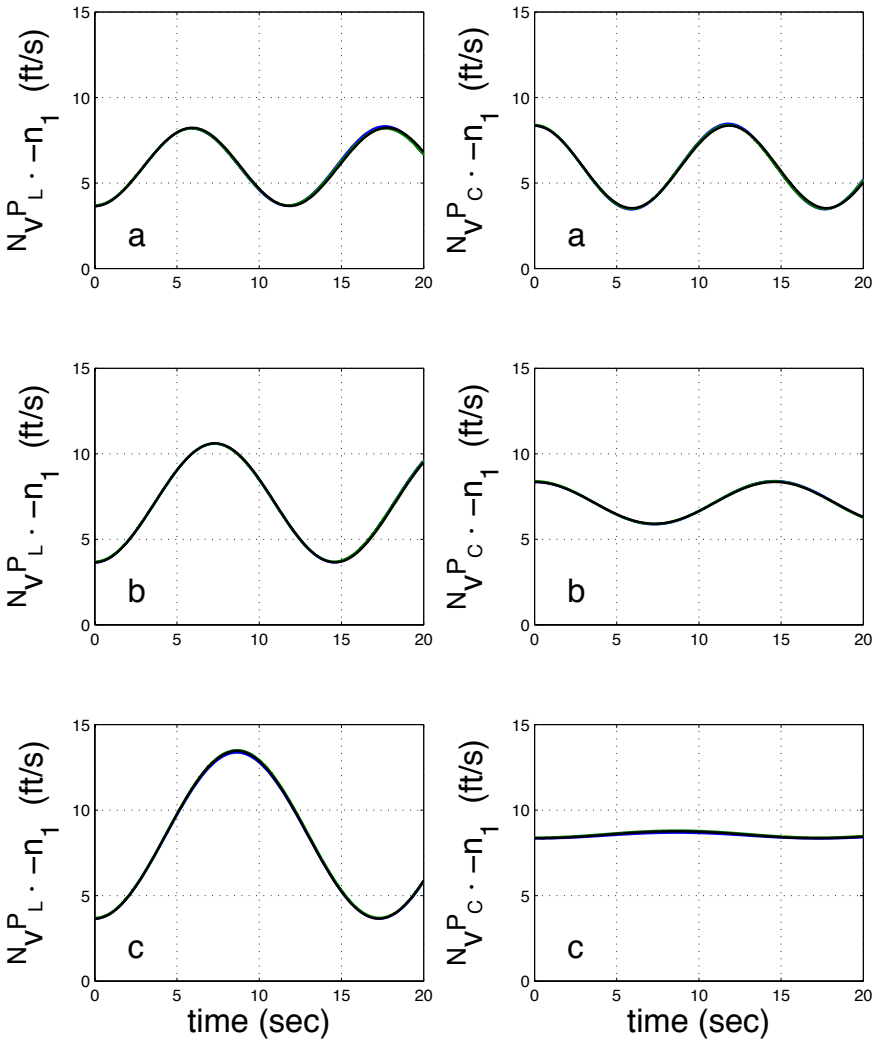

Figure 11. Capsule and Parachute Speeds, Eastward. Capsule (left), Parachute (right). Dumbbell model (black), CAPDYN results (blue), FAST results (green).

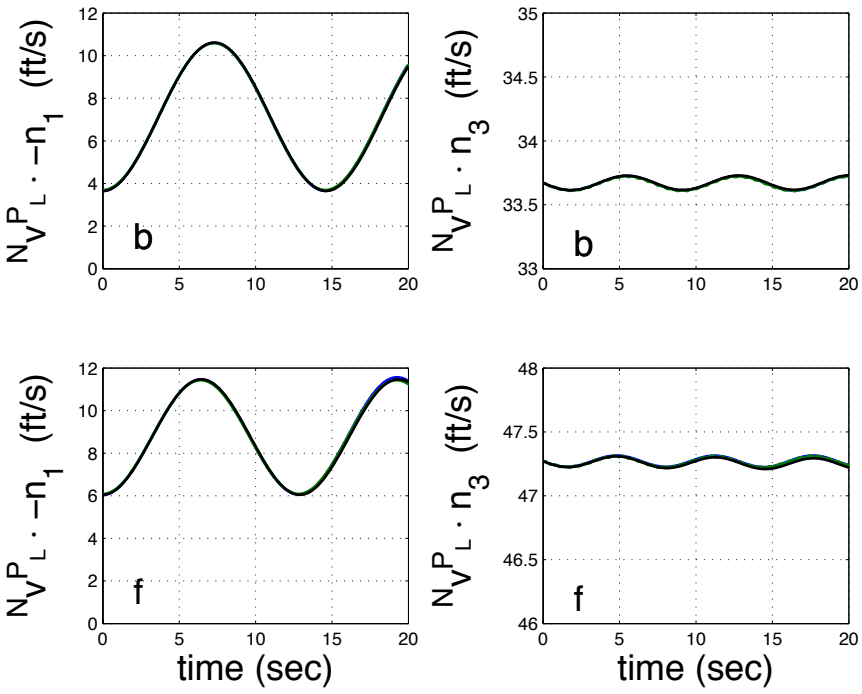

Figure 12. Capsule Speeds, Eastward and Downward. Eastward (left), Downward (right). Dumbbell model (black), CAPDYN results (blue), FAST results (green).

Inspection of Eq. (41) shows that decreasing the parachute drag coefficient C_A causes the pivot point to move towards the capsule. A comparison of cases b and f in Table 3 reveals that when $C_{N_\alpha} = 0.3$, reducing C_A from 0.85 to 0.425 changes L_L from 174 ft to 136 ft. Figure 12 provides plots of $-{}^N\mathbf{v}^{P_L} \cdot \hat{\mathbf{n}}_1$ on the left side. The results shown in Fig. 12 are consistent with the conclusion drawn in Refs. [2], [5], and [6] that the static stability of a parachute can be enhanced by increasing its porosity. However, even though the amplitude of oscillation in eastward speed is reduced somewhat by reducing C_A, the maximum is higher for $C_A = 0.425$, which is counterproductive. Of course, a reduction in C_A leads to a higher descent speed (and dynamic pressure), as indicated on the right side of Fig. 12. It is worth noting that, according to Eq. (41), increasing the capsule mass (which increases W_{tot}) has the same effect as decreasing C_A.

V. Conclusions

A significant amount of insight into pendulum motion of a capsule supported by two parachutes is obtained by modeling the system as a simple dumbbell performing planar motion. An analytical investigation of the dynamics of pendulum motion is undertaken by assuming that parachute normal force coefficient is a linear function of angle of attack in the neighborhood of a stable equilibrium point. For small-amplitude oscillations, the equation of motion for swing angle is found to have the form of the second-order linear differential equation governing damped, free vibrations, and a general solution of the differential equation is given. A point on the dumbbell whose trajectory is nearly a straight line for undamped, small-amplitude oscillations is identified and referred to as the pivot point. The main contribution of the paper is the development of an analytical relationship for the location of the pivot point. Inspection of the analytical relationship reveals the distance from the payload to the pivot point, which should be minimized, can be reduced by increasing parachute normal force coefficient slope at the trim angle of attack, increasing payload mass, decreasing axial force coefficient (at the expense of increasing descent speed), and decreasing the mass of the air entrapped in a parachute. The practical implication of the last observation is that pendulum motion is exacerbated as the system descends and air density increases. All of these conclusions based on the analytical relationship are consistent with existing literature.

VI. Acknowledgments

The work reported here was performed as part of an effort undertaken by the NASA Engineering and Safety Center. The authors would like to express their gratitude to other members of the NESC parachute assessment team for providing helpful information and insights: Paul Tartabini, Dan Murri, Mike Mendenhall, Dr. Eugene Morelli, Tuan Truong, and Ricardo Machín.

References

[1]Ray, E. S., and Machín, R. A., "Pendulum Motion in Main Parachute Clusters," No. 2015-2138, AIAA, 2015.

[2]White, F. M., and Wolf, D. F., "A Theory of Three-Dimensional Parachute Dynamic Stability," *Journal of Aircraft*, Vol. 5, No. 1, 1968, pp. 86–92.

[3]Ginn J. M., Clark, I. G., and Braun, R. D., "Parachute Dynamic Stability and the Effects of Apparent Inertia," No. 2014-2390, AIAA, 2014.

[4]Eaton, J. A., "Added Mass and the Dynamic Stability of Parachutes," *Journal of Aircraft*, Vol. 19, No. 5, 1982, pp. 414–416.

[5]Knacke, T. W., *Parachute Recovery Systems Design Manual*, Para Publications, Santa Barbara, 1991.

[6]Greathouse, J. S., and Schwing, A. M., "Study of Geometric Porosity on Static Stability and Drag using Computational Fluid Dynamics for Rigid Parachute Shapes," No. 2015-2131, AIAA, 2015.

[7]Ali, Y., Sommer, B., Truong, T., Anderson, B., and Madsen, C., "Orion Multi-Purpose Crew Vehicle Solving and Mitigating the Two Main Cluster Pendulum Problem," No. 2017-4056, AIAA, 2017.

[8]Kane, T. R., and Levinson, D. A., *Dynamics: Theory and Applications*, McGraw-Hill, New York, 1985, pp. 158–159.

[9]Pamadi, B. N., *Performance, Stability, Dynamics, and Control of Airplanes*, 3rd Ed., AIAA, 2015, pp. 427–428.

[10]Morelli, E. A., and Klein, V., *Aircraft System Identification, Theory and Practice*, Sunflyte Enterprises, Williamsburg, VA., 2016, pp. 56–57.